Inorganic Chemistry

Article

pubs.acs.org/IC

Synthesis and Size Control of Iron(II) Hexacyanochromate(III) Nanoparticles and the Effect of Particle Size on Linkage Isomerism

Matthieu F. Dumont,[†,‡,⊥] Olivia N. Risset,[†] Elisabeth S. Knowles,[‡] Takashi Yamamoto,[†,§] Daniel M. Pajerowski,[‡,∥] Mark W. Meisel,*[,‡] and Daniel R. Talham*[,†]

[†]Department of Chemistry, University of Florida, Gainesville, Florida 32611-7200, United States

[‡]Department of Physics and the National High Magnetic Field Laboratory, University of Florida, Gainesville, Florida 32611-8440, United States

[§]Department of Chemistry, Keio University, 3-14-1 Hiyoshi, Yokohama, 223-8522, Japan

Supporting Information

ABSTRACT: The controlled synthesis of monodisperse nanoparticles of the cubic Prussian blue analogue iron(II) hexacyanochromate(III) is reported along with a kinetic study, using cyanide stretching frequencies, showing the variations of the activation energy (E_a) of the linkage isomerism as a function of the particle size. Highly reproducible, cubic-shaped iron(II) hexacyanochromate(III) nanocrystals, with sizes ranging from 2 to 50 nm, are synthesized using a microemulsion technique, whereas a bulk synthesis yields nonuniform less monodisperse particles with sizes greater than 100 nm. Monitoring the cyanide stretching frequency with FTIR spectroscopy shows that the rate of isomerization is faster for smaller particles. Moreover, a kinetic analysis at different temperatures (255 K ≤ T ≤ 321 K) gives insight into the evolution of E_a with the particle size. Finally, time-dependent powder X-ray diffraction and net magnetization confirm the FTIR observations. The data are interpreted within the concept of a simple two-component model with different activation energies for structures near the surface of the solid and within the bulk.

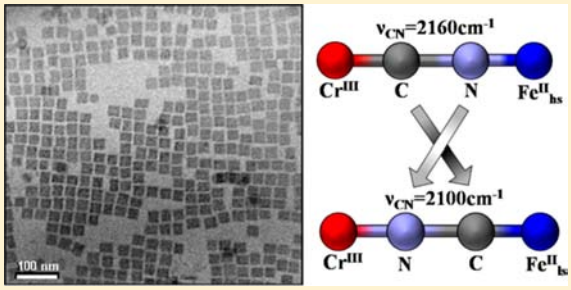

INTRODUCTION

Prussian blue, a face-centered cubic network of iron(III) ions bridged by ferrocyanide ions, has been extensively studied for its fundamental inorganic chemistry as well as for potential applications, including electrochromics,[1−3] heavy-metal sequestration,[4,5] and hydrogen peroxide detection.[6,7] By replacing one or more of the iron centers by other transition metals, a wide variety of coordination polymers can be synthesized, and such compounds are called Prussian blue analogues (PBAs). In the extended PBA family, some analogues display intriguing properties such as room-temperature magnetism,[8,9] photomagnetism,[10−16] electrochromism,[17] photochromism,[18,19] and spin-crossover effects.[18,20,21] Due to the somewhat softer nature of coordination polymers relative to traditional ionic and elemental solids, changes in temperature, pressure, and irradiation can induce structural and sometimes chemical modifications that lead to dramatic changes in the physical properties.[11−15,18,20−29]

An intriguing example is linkage isomerism, which refers to the different ways a ligand bridges to two metal centers, for example, in the case of cyanide giving either M−CN−M′ or M−NC−M′ isomers (Figure 1). Linkage isomerism was first observed in iron(II) hexacyanochromate(III) more than 40 years ago,[30,31] but this interesting phenomenon continues to attract attention.[23,24,32] In the case of iron(II) hexacyanochromate(III), the cyanide bond will "turn over", switching from the as-synthesized Cr^{III}−CN−Fe^{II}_{HS} to give the more stable Cr^{III}−NC−Fe^{II}_{LS}. The change in coordination environment results in a change of the ligand field strength around the Fe^{II} center, thus inducing a spin-state transition. The high-spin state in the original isomer, with the nitrogen atom bound to Fe^{II}, switches to a low-spin state where Fe^{II} coordinates to the carbon end. Literature precedent showed the linkage isomerism to be reversible as a function of the pressure applied on the network but irreversible after X-ray illumination or thermal cycling.[20,21,23,24,33,34] In 2005, Coronado et al.[24] reported the pressure dependence of the phenomenon in iron hexacyanochromate, establishing a direct relationship between pressure and the extent of the linkage isomerism. The changes in coordination associated with the linkage isomerism lead to contraction of the lattice from 10.65 to 10.05 Å, inducing distortions in the three-dimensional network.

There is currently great interest in exploring the chemical and physical properties of coordination polymers in the nanometer-size regime and comparing them to their corresponding bulk properties.[35−39] Arai et al.[32] compared the Fourier-transform infrared (FTIR) spectrum of bulk iron(II)

Received: December 17, 2012
Published: April 4, 2013

   dx.doi.org/10.1021/ic302764k | Inorg. Chem. 2013, 52, 4494−4501

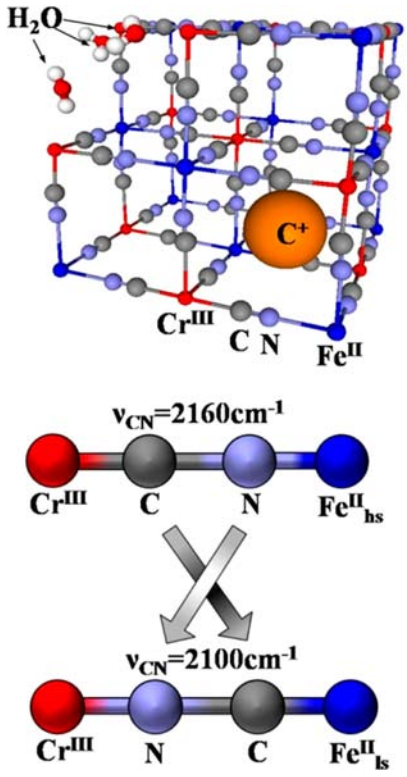

Figure 1. Top: unit cell of a PBA showing the vacancies and cations necessary to balance the charge. The cubic geometry gives the shape to the crystals. Bottom: scheme depicting the linkage isomerism and the effect on the FTIR cyanide stretching frequencies.

hexacyanochromate(III) to that of nanoparticles of the same material stabilized with 4-(dioctadecylamino)pyridine. They observed that, a month after synthesis, the FTIR band corresponding to isomerized material became more intense for iron hexacyanochromate nanoparticles than for the bulk material. Consequently, the authors conjectured that linkage isomerism is easier in the nanoparticles because of the difference in lattice energy caused by the stabilizing ligand on the nanoparticle surface.[32] Similar observations were reported by House and Kob[40] for cadmium hexacyanoferrate, for which the rate of isomerization was found to be inversely proportional to the size of the particles. Each of these studies compared nanoparticles to the bulk, but to our knowledge, no study of the effect of particle size on linkage isomerism has been reported.

In this Article, the controlled synthesis of monodisperse cubic iron(II) hexacyanochromate(III) nanocrystals using a microemulsion technique is described, followed by a kinetic study, based on cyanide stretching frequencies, showing the variations of the activation energy (E_a) of the linkage isomerism as a function of the particle size. The extracted activation energies are consistent with time-dependent structural and magnetic studies. The results show that the linkage isomerization rate increases as the particles become smaller. A simple model is applied to predict the rates for different particle sizes, using surface to volume ratios and different values of E_a for surface and bulk regions.

EXPERIMENTAL SECTION

General Remarks. $K_3[Cr^{III}(CN)_6]\cdot nH_2O$ was synthesized via literature routes.[41] ***Caution!*** *Potassium cyanide (KCN) is highly toxic and should be handled with care.* Deionized water used in the synthetic procedures was obtained from a Barnstead NANOpure system with a resistivity of at least 17.8 MΩ cm. All of the other reagents were purchased from Sigma-Aldrich or Fisher-Acros and used without further purification.

$K_{0.5}Fe_4[Cr(CN)_6]_{2.8}\cdot 7.2H_2O$ (1). A solution of 60 mg of $K_3Cr(CN)_6$ in 4 mL of H_2O was added to 80 mL of cyclohexane under vigorous stirring, followed by dropwise addition of 27 mg of $FeCl_2$ in 4 mL of H_2O over 5 min. After 10 min the precipitate was collected by centrifugation and washed with 15 mL of water and 2 × 15 mL of acetone. FTIR (KBr): 2160 (s, ν_{CN}), 2100 (m, ν_{CN}) cm^{-1}. EDS (Fe:Cr): 58.8:41.2. Anal. Calcd for $C_{4.2}H_{3.6}N_{4.2}O_{1.8}K_{0.1}Fe_{1.0}Cr_{0.7}$: C, 21.2; H, 1.5; N, 24.7. Found: C, 21.7; H, 1.3; N, 24.6.

$K_{0.2}Fe_4[Cr(CN)_6]_{2.6}\cdot 7.8H_2O$ 50 nm Nanocrystals (2). Nanocrystals were obtained by adding 60 mg of $K_3Cr(CN)_6$ in 4 mL of H_2O to a solution of IGEPAL CO-520 (10 mL) dissolved in 80 mL of cyclohexane under vigorous stirring. A solution of 22 mg of $FeCl_2$ in 4 mL of H_2O was then added dropwise to the mixture over 5 min. To facilitate the workup, the solvent volume was increased by adding 40 mL of cyclohexane. After 10 min, the microemulsion was broken with 30 mL of acetone. The nanoparticles were collected by centrifugation and washed with 15 mL of water and 2 × 15 mL of acetone. FTIR (KBr): 2160 (s, ν_{CN}), 2100 (m, ν_{CN}) cm^{-1}. EDS (Fe:Cr): 60.6:39.3. Anal. Calcd for $C_{3.9}H_{4.2}N_{3.9}O_{2.1}K_{0.0}Fe_{1.0}Cr_{0.6}$: C, 20.4; H, 1.8; N, 23.8. Found: C, 19.9; H, 1.3; N, 24.6.

$K_{0.8}Fe_4[Cr(CN)_6]_{2.9}\cdot 6.6H_2O$ 30 nm Nanocrystals (3). The same procedure was followed as for the preparation of **2** except that 16 mL of IGEPAL CO-520 was used and 100 mg of KCl was added to the solution of $FeCl_2$. FTIR (KBr): 2160 (s, ν_{CN}), 2100 (m, ν_{CN}) cm^{-1}. EDS (Fe:Cr): 57.9:42.0. Anal. Calcd for $C_{4.3}H_{3.3}N_{4.3}O_{1.6}K_{0.2}Fe_{1.0}Cr_{0.7}$: C, 21.5; H, 1.3; N, 25.1. Found: C, 21.8; H, 1.6; N, 24.9.

$K_{1.1}Fe_4[Cr(CN)_6]_{3.0}\cdot 6.0H_2O$ 30 nm Nanocrystals (4). The same procedure was followed as for the preparation of **3**. FTIR (KBr): 2160 (s, ν_{CN}), 2100 (m, ν_{CN}) cm^{-1}. EDS (Fe:Cr): 57.1:42.8. Anal. Calcd for $C_{4.5}H_{3.0}N_{4.5}O_{1.5}K_{0.3}Fe_{1.0}Cr_{0.7}$: C, 21.7; H, 1.2; N, 25.4. Found: C, 20.9; H, 1.0; N, 24.8.

$K_{1.4}Fe_4[Cr(CN)_6]_{3.1}\cdot 5.4H_2O$ 30 nm Nanocrystals (5). The same procedure was followed as for the preparation of **3** except that 250 mg of KCl was added to the solution of $FeCl_2$. FTIR (KBr): 2160 (s, ν_{CN}), 2100 (m, ν_{CN}) cm^{-1}. EDS (Fe:Cr): 56.3:43.6. Anal. Calcd for $C_{4.6}H_{2.7}N_{4.6}O_{1.3}K_{0.3}Fe_{1.0}Cr_{0.77}$: C, 22.0; H, 1.0; N, 25.6. Found: C, 21.7; H, 1.1; N, 25.1.

$K_{1.8}Fe_4[Cr(CN)_6]_{3.2}\cdot 4.8H_2O$ 30 nm Nanocrystals (6). The same procedure was followed as for the preparation of **3** except that 250 mg of KCl was added to the solution of $FeCl_2$. FTIR (KBr): 2160 (s, ν_{CN}), 2100 (m, ν_{CN}) cm^{-1}. EDS (Fe:Cr): 55.5:44.4. Anal. Calcd for $C_{4.8}H_{2.4}N_{4.8}O_{1.2}K_{0.4}Fe_{1.0}Cr_{0.8}$: C, 22.1; H, 0.9; N, 25.8. Found: C, 21.8; H, 1.0; N, 25.3.

$K_{0.2}Fe_4[Cr(CN)_6]_{2.7}\cdot 7.8H_2O$ 30 nm Nanocrystals (7). The same procedure was followed as for the preparation of **3** except that no KCl was added to the solution of $FeCl_2$. FTIR (KBr): 2160 (s, ν_{CN}), 2100 (m, ν_{CN}) cm^{-1}. EDS (Fe:Cr): 59.7:40.2. Anal. Calcd for $C_{4.0}H_{3.9}N_{4.0}O_{1.9}K_{0.0}Fe_{1.0}Cr_{0.6}$: C, 20.9; H, 1.6; N, 24.4. Found: C, 19.6; H, 1.6; N, 24.3.

$K_{0.2}Fe_4[Cr(CN)_6]_{2.7}\cdot 7.8H_2O$ 2 nm Nanocrystals (8). Nanocrystals were obtained by adding 60 mg of $K_3Cr(CN)_6$ in 4 mL of H_2O to a solution of IGEPAL CO-520 (35 mL) dissolved in 80 mL of cyclohexane under vigorous stirring. A solution of 22 mg of $FeCl_2$ in 4 mL of H_2O was then added dropwise to the mixture over 5 min. To facilitate the workup, the solvent volume was increased by adding 40 mL of cyclohexane. After 10 min, the microemulsion was broken with 150 mL of acetone. The nanoparticles were collected by centrifugation at 3200 rpm. Due to the great amount of surfactant present in the solution, extensive washing was necessary to isolate the particles for imaging. The nanocrystals were washed with 4 × 30 mL of acetone, 5 × 30 mL of water, 5 × 30 mL of acetone/water (1:1), and finally 1 × 30 mL of acetone. FTIR (KBr): 2160 (s, ν_{CN}), 2150 (sh, terminal CN), 2100 (m, ν_{CN}) cm^{-1}. Considering the unknown amount of surfactant present in the final product, elemental analysis was performed to determine the Fe:Cr ratio. Anal. Calcd for $C_{4.0}H_{3.9}N_{4.0}O_{1.9}K_{0.0}Fe_{1.0}Cr_{0.7}$: Fe:Cr = 1.58. Found: Fe:Cr = 1.58.

dx.doi.org/10.1021/ic302764k | Inorg. Chem. 2013, 52, 4494−4501

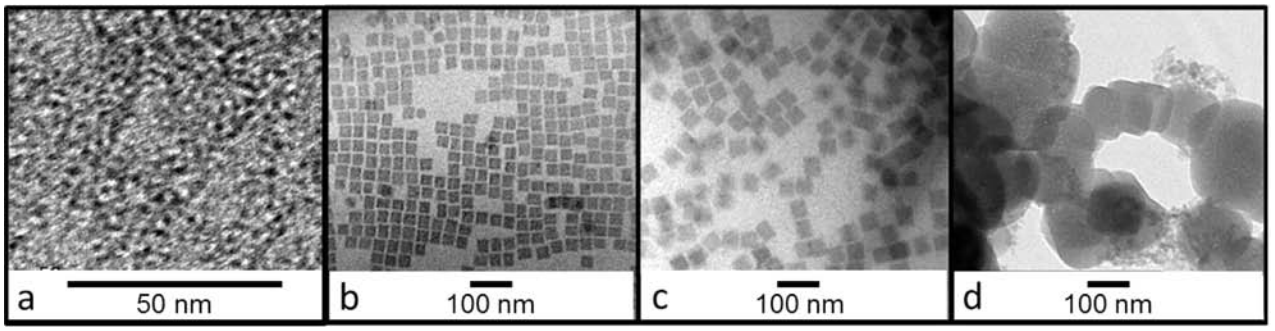

Figure 2. HRTEM images of the four different sizes of particles: (a) 2 nm nanocrystals (**8**), (b) 30 nm nanocrystals (**3**), (c) 50 nm nanocrystals (**2**), and (d) bulk material (**1**). Scale bars represent 100 nm.

Characterization. Combustion analyses to determine carbon, hydrogen, and nitrogen (CHN) percentages were performed by the University of Florida Spectroscopic Services laboratory. Combustion analyses to determine iron and chromium percentages were performed at Complete Analysis Laboratories, Inc. (Parsippany, NJ). Transmission electron microscopy was performed on a JEOL-2010F HRTEM instrument at 200 kV. TEM grids (carbon film on a holey carbon support film, 400 mesh, copper from Ted-Pella, Inc.) were prepared by dropping, onto the grid, 20 μL of a solution containing 5 mg of sample dispersed by sonication in 2 mL of EtOH for 30 s. Energy dispersive X-ray spectroscopy (EDS) was performed with an Oxford Instruments EDS X-ray microanalysis system coupled to the HRTEM microscope. A total of four scans were performed on different parts of the TEM grid and then averaged to give relative atomic percentages for chromium and iron. The Fe:Cr atomic ratios were similar within experimental error in the different locations, which confirms the uniformity of the sample. Chemical formulas are based on the metal composition from EDS, adding water and potassium as determined by the number of trivalent metal vacancies to ensure electroneutrality.

Physical Measurements. Powder samples, typically 10−15 mg, were immobilized in a gelatin capsule that was secured in a plastic drinking straw for loading in a SQUID magnetometer (Quantum Design MPMS-XL7). Isothermal magnetization was measured at 5 K while the field was swept between 0 and 70 kG. Subsequently, data were obtained during warming to 300 K in an applied field of 100 G.

Powder X-ray diffraction (PXRD) data were obtained using a Philips APD 3720 powder diffractometer using Cu Kα radiation with a wavelength of 0.154184 nm. A 100 mg sample of nanoparticles was mounted on double-sided tape backed by a glass slide.

Infrared spectra were recorded on a Nicolet 6700 Thermo Scientific spectrophotometer. Typically 64 scans were taken between 2200 and 1900 cm^{-1} with a precision of 0.482 cm^{-1}. Powder samples were mixed with KBr and pressed into a pellet using 20 MPa, noting that pressure effects on linkage isomerism start to be detectable at 320 MPa and are significant at 670 MPa.[23,24] A scan of pure KBr was taken as a background reference. For the kinetic studies, the sample was divided into three portions stored at 255, 298, and 321 K immediately after isolation of the compound. An FTIR spectrum of each fraction was taken at regular periods of time for 3 h.

RESULTS

Sample Synthesis and TEM Analysis. The effect of IGEPAL CO-520 on the formation of $K_jFe^{II}_k[Cr^{III}(CN)_6]_l \cdot nH_2O$ nanoparticles was established with transmission electron microscopy. Nanoparticles were formed in a water-in-oil reverse microemulsion,[42,43] varying the amount of surfactant from 10 to 35 mL for 80 mL of cyclohexane to control the particle size. HRTEM images of these samples revealed cubic nanoparticles (Figure 2). The mean face diagonals were 2 nm (**8**), 30 nm (**3**), and 50 nm (**2**) for the samples prepared with 35, 16, and 10 mL of IGEPAL, respectively.

Bulk samples of iron(II) hexacyanochromate(III) were prepared following the procedure described by House and Bailar.[31] Upon dropwise addition of the precursors under vigorous stirring, a brick orange precipitate slowly appeared, suggesting the formation of $K_jFe^{II}_k[Cr^{III}(CN)_6]_l \cdot nH_2O$. HRTEM images (Figure 2) showed a tendency toward cubic-shaped particles, although the shapes were not uniform. The average particle size was larger than 100 nm.

PXRD, Magnetization, and FTIR Measurements. Linkage isomerism occurs with a significant contraction of the unit cell parameter a from 10.65 to 10.05 Å associated with the spin-state transition.[30] Coronado et al.[23,24] observed that the lattice parameter a decreases in a linear fashion with a decrease in the percentage of chromium cyanide bonds. Monitoring the linkage isomerism with PXRD over a period of 10 days, the shift in peak position was faster for the 30 nm nanoparticles than for the bulk (Figure 3). The extent of isomerization was estimated using the mean value of a, calculated from the [400] reflections. After 10 days, the number of isomerized cyanide bonds stabilized at 36% total conversion for the bulk and 42% total conversion for the nanoparticles. Practically, significant conversion takes place before the samples are effectively isolated for initial measurements. Figure 4 shows, for example, that by PXRD the extent of conversion between the first measurement following isolation of the samples (0 h) and 96 h is 3.6 ± 0.6% for the bulk and 9.9 ± 0.9% for the 30 nm particles (Figure 4).

For the magnetization studies, data were acquired immediately following the synthesis (t < 15 min) and after 4 days. The ligand-induced transition from Fe^{II}_{HS} (S = 2) to Fe^{II}_{LS} (S = 0) associated with the linkage isomerism leads to a modification of the magnetic behavior as evidenced by the isothermal (T = 5 K) field-dependent magnetization (Supporting Information).[23,33,44] On the basis of the values of the magnetization at saturation, the percentage of isomerized material was calculated to be 5 ± 0.06% for the bulk and 9 ± 0.07% for the 30 nm nanoparticles, consistent with the values observed by PXRD (Figure 4). Coercivity in magnetization as a function of the applied field also evolved as the linkage isomerization progressed, along with a decrease in T_c, and these changes occurred faster for the nanoparticles than for the bulk (Supporting Information).

In addition, the percentage of isomerized cyanide linkages after 91 h was determined by integrating the FTIR band at 2160 cm^{-1} (Fe^{II}_{HS}−NC−Cr) (Supporting Information), providing an estimate of the extent of isomerization: 6 ± 2% for the bulk and 11 ± 2% for the 30 nm particles. These results further indicate faster isomerization rates as well as a greater

dx.doi.org/10.1021/ic302764k | Inorg. Chem. 2013, 52, 4494−4501

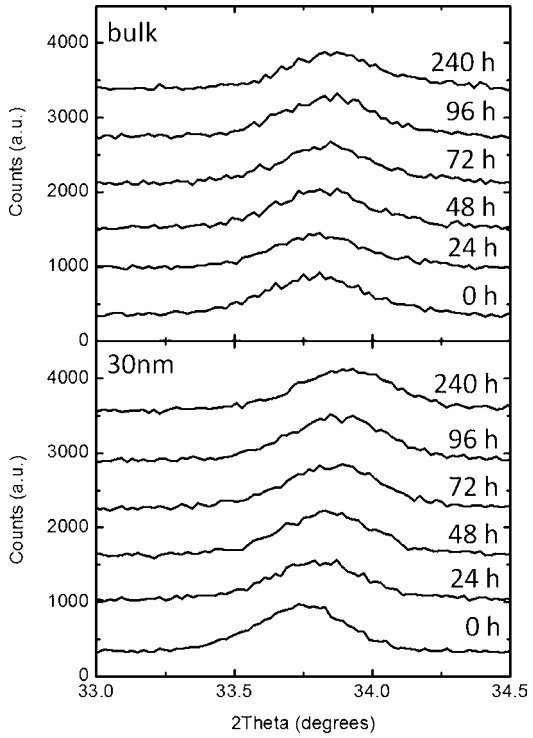

Figure 3. Time evolution over 240 h of the PXRD pattern around the angle corresponding to the [400] reflections for the bulk sample (**1**) (top) and 30 nm nanocrystals (**7**) (bottom) at room temperature. Time 0 h corresponds to the time of the first measurement, taken immediately upon isolation of the sample.

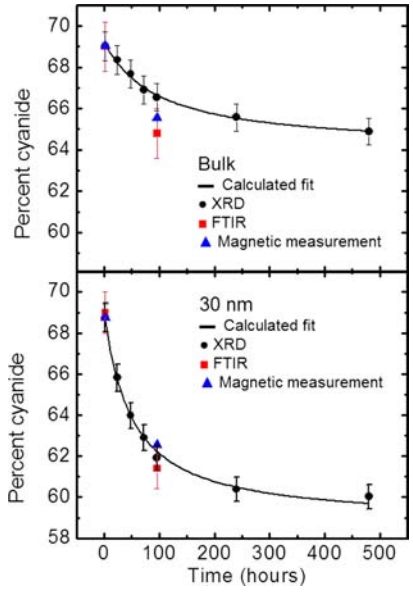

Figure 4. Time evolution of the percentage of the chromium cyanide for the bulk sample (**1**) (top) and 30 nm nanocrystals (**7**) (bottom). Black circles indicate the percentage of cyanide derived from PXRD, the red squares that from FTIR, and the blue triangles (with error bars contained in the symbol) that from magnetic measurements (see the Supporting Information). The black lines are theoretical predictions generated using Supporting Information eq 4 and the parameters in Supporting Information Table S1. Time 0 h corresponds to the time of the first measurement, taken immediately upon isolation of the sample.

extent of the isomerization in the nanoparticles compared to the bulk (Figure 4).

Kinetic Analysis of the Linkage Isomerism. To follow the linkage isomerism, FTIR spectra of each sample were recorded as a function of time at three different temperatures (Figure 5). The growth of a distinct band at 2100 cm^{-1} indicates the isomerization of the cyanide bond from Cr^{III}–CN–Fe^{II}_{HS} to Cr^{III}–NC–Fe^{II}_{LS}. Linkage isomerism and the associated spin transition of Fe^{II} from HS ($t_{2g}^4e_g^2$) to LS ($t_{2g}^6e_g^0$) modifies the π back-bonding, resulting in a shift of the CN stretching band to lower energy.[32,45] The FTIR shift of approximately 60 cm^{-1} provides a local probe. As shown in Figure 5, the changes are more pronounced for smaller particles than for the bulk solid. The IR spectra for the 2 nm particles exhibit an additional shoulder at 2150 cm^{-1} attributed to terminal cyanides that do not undergo linkage isomerism.

According to previous work by House and Bailar,[31] the reaction rates were determined on the basis of linear fits of the ratio of isocyanide to cyanide plotted as a function of time (Figure 6). The peak area of the chromium isocyanide band increases more dramatically than the area of the cyanide band decreases because of the different molar absorption coefficients of the two types of linkages. For each spectrum, the bands were integrated by fitting the peaks to Lorentzian lines, and the different extinction coefficients were accommodated by by plotting the isocyanide:cyanide band intensity ratios.

From the measured rates at different temperatures, the activation energy for each particle size was determined using the Arrhenius equation, $k = Ae^{-E_a/RT}$, where k is the rate constant, A is the pre-exponential factor; E_a is the activation energy, R is the gas constant, and T is the temperature. Applying the Arrhenius law, E_a = 46 kJ·mol^{-1} was found in the bulk material, which is larger than those determined for smaller particle sizes (Table 1). The value of E_a decreased from 28 to 22 kJ·mol^{-1} and reached 11 kJ·mol^{-1} for 50, 30, and 2 nm nanoparticles, respectively. Interestingly, the activation energy is nearly independent of the composition for the different formulas studied (Table 1).

DISCUSSION

The FTIR kinetic studies of the linkage isomerism in iron hexacyanochromate show that the rate of isomerization increases as the particle size decreases. There is, now, common understanding that the properties of a material can be subject to change as the size approaches the nanoscale. Putting quantum confinement effects aside,[46] as the surface to volume ratio becomes significant, properties intrinsic to the surface of the particle can modify or overcome the bulk properties. The ability to synthesize monodisperse nanoparticles in a wide range of sizes is critical to map behavior within the nanoregime and at its boundaries. In the area of coordination polymers there has been a significant focus on generating and stabilizing PBA nanoparticles. A popular approach consists in controlling size by taking advantage of the spatial confinement of the precursors, which can be achieved by using polymers or by performing the synthesis in supramolecular structures such as reverse micelles.[35,47−50] The resulting smaller particles are very uniform in size and shape (Figure 2). The monodispersity decreases as the amount of surfactant diminishes to achieve larger particles. It is interesting that variation of the ionic composition does not seem to have a noticeable influence on the surfactant ability to affect the size control of the particles (Table 1).

Forty years ago, Brown et al.[30] reported an E_a of 17 kcal·mol^{-1} (71 kJ·mol^{-1}) based on magnetic susceptibility

dx.doi.org/10.1021/ic302764k | Inorg. Chem. 2013, 52, 4494−4501

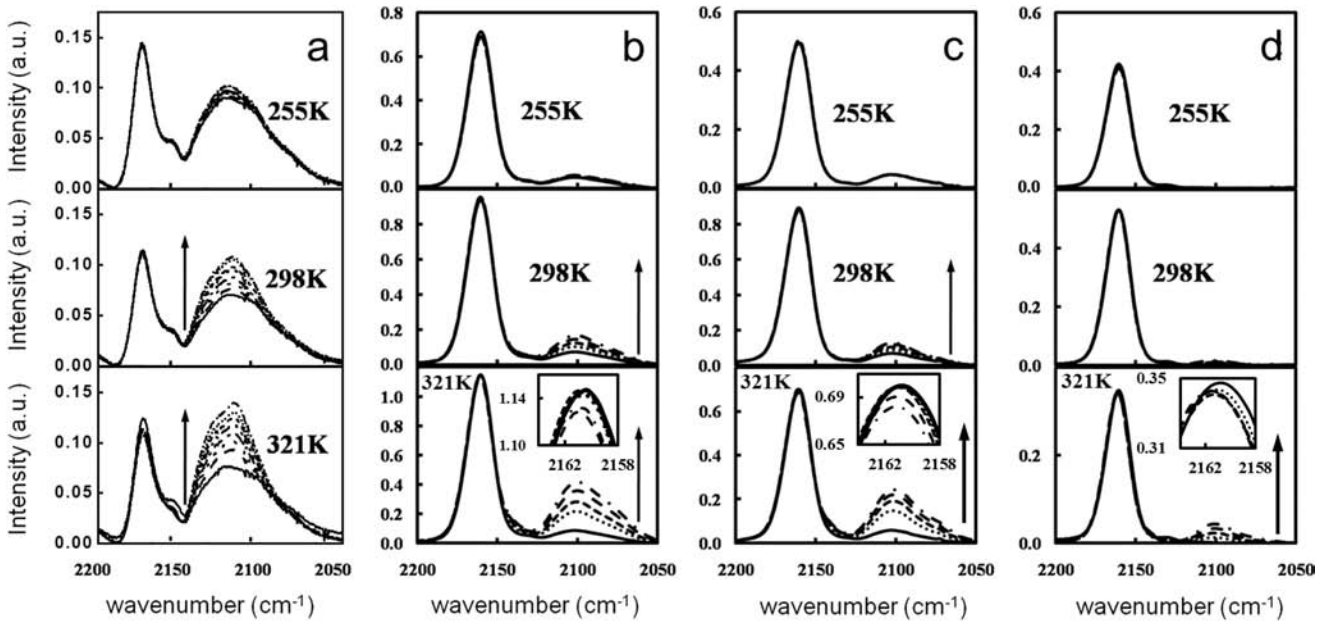

Figure 5. Time evolution over 3 h of the FTIR spectra for each size of particles at different temperatures (255, 298, and 321 K): (a) 2 nm nanocrystals (**8**), (b) 30 nm nanocrystals (**3**), (c) 50 nm nanocrystals (**2**), and (d) bulk material (**1**).

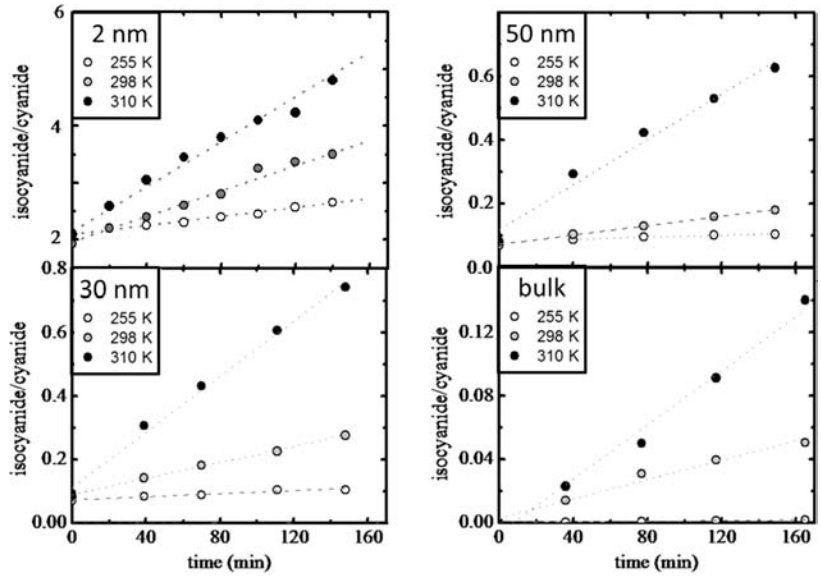

Figure 6. Evolution of the isocyanide (Fe−CN−Cr):cyanide (Fe−NC−Cr) ratio vs time for 2 nm nanoparticles (**8**) (top left), 30 nm nanocrystals (**3**) (bottom left), 50 nm nanocrystals (**2**) (top right), and the bulk sample (**1**) (bottom right). The linear fits (dashed line) give the rate constant, *k*.

measurements, while, almost simultaneously, House and Bailar, using FTIR spectroscopy, estimated E_a = 24.1 kcal·mol^{-1} (100.8 kJ·mol^{-1}) for the bulk material.[31] These earlier studies included measurements at higher temperatures, where it is now understood that other processes such as partial oxidation and spin crossover also occur concurrently with the linkage isomerism,[23,30] likely accounting for differences with the current study. The present study focuses on initial kinetic regimes at lower temperatures to only monitor the processes with the lower thermodynamic barrier. More recently, Kob and House reported an activation energy of 28.7 kJ·mol^{-1} for cyanide linkage isomerism in a silver hexacyanocobaltate analogue.[51]

Similarities exist between the linkage isomerism phenomenon and lattice-energy-driven structural phase transitions since both involve reorganization of the solid, including atom rearrangement and changes in the lattice parameters. Typically, solid−solid phase transitions nucleate at defects.[52] The transition of a whole domain from one phase to another applies mechanical stress on contiguous domains, creating new defects, which themselves generate new transitioning domains. Studies of phase transitions in nanometer-sized particles of zinc sulfide have shown that activation energies are greater in the nanoparticles than in bulk compounds of the same composition.[53] In nanoparticles, the smaller scale reduces the number of domains and allows for potentially higher crystallinity, making the ratio of defects per volume unit smaller than in the bulk. Also, any mechanical strain can only be propagated to a discrete particle, so the amount of material

dx.doi.org/10.1021/ic302764k | Inorg. Chem. 2013, 52, 4494−4501

Table 1. Chemical Formula and Activation Energy for the Linkage Isomerism of Iron(II) Hexacyanochromate(III) Particles

chemical formula[a]	compd	particle size[b] (nm)	E_a[c] (kJ·mol^{-1})
$K_{0.5}Fe_4[Cr(CN)_6]_{2.8}\cdot 7.2\ H_2O$	**1**	110 ± 25	46 ± 3
$K_{0.2}Fe_4[Cr(CN)_6]_{2.6}\cdot 7.8\ H_2O$	**2**	51 ± 3.6	28 ± 2
$K_{0.8}Fe_4[Cr(CN)_6]_{2.9}\cdot 6.6\ H_2O$	**3**	29 ± 3.1	22
$K_{1.1}Fe_4[Cr(CN)_6]_{3.0}\cdot 6.0\ H_2O$	**4**	29 ± 3.1	21[d]
$K_{1.4}Fe_4[Cr(CN)_6]_{3.1}\cdot 5.4\ H_2O$	**5**	29 ± 3.1	20[d]
$K_{1.8}Fe_4[Cr(CN)_6]_{3.2}\cdot 4.8\ H_2O$	**6**	29 ± 3.1	20[d]
$K_{0.2}Fe_4[Cr(CN)_6]_{2.7}\cdot 7.8\ H_2O$	**7**	29 ± 3.1	23 ± 2
$K_{0.2}Fe_4[Cr(CN)_6]_{2.7}\cdot 7.8\ H_2O$	**8**	2 ± 1	11 ± 1

[a]Determined by EDS, ICP-MS, and elemental analysis. [b]Determined from TEM pictures. [c]The uncertainty in E_a is ±1.5 kJ·mol^{-1} unless otherwise stated. [d]Calculated on the basis of the value of k at 298 K.

potentially affected by a single defect decreases with smaller particles.[54−56]

Due to the nonstoichiometric nature of PBAs, the main class of defects is cyanometallate vacancies. Adjacent to the vacancies, the structure is less constrained, making atom rearrangement easier (Figure 1). In addition, the coordinated water molecules lower the local ligand fields, lowering the energy gap for spin crossover or metal to metal charge transfer events that are intimately related to the linkage isomerism mechanism.[23,24,44,57] To study the impact of the number of defects independently of the size of the particles, we synthesized 30 nm nanocrystals with different compositions. Metal ratios were varied by increasing the concentration of potassium during the synthesis. The high concentration of interstitial cations modifies the charge balance during the formation of the crystals, leading to a smaller number of hexacyanochromate vacancies. The activation energies for the particles with different compositions are presented in Table 1. Somewhat surprisingly, the values of E_a remain the same, even over a wide range of lattice composition. Therefore, the difference in the extent of vacancies, or lattice defects, does not explain the change in activation energy observed while the particle size is varied.

The results suggest that the rate of linkage isomerism is related to the surface to volume ratio and the notion that the process is easier at the surface. In the semirigid coordination polymer environment, due to the smaller number of adjacent lattices to distort, structural changes on the surface of the particle are expected to require less energy than in the core. The surface structure differs from the bulk structure, and as with metallic and ionic solids, such distortions can propagate into the bulk for some distance to minimize the energy of the structural change, although for coordination polymers there is certainly much less known about the depth of surface reorganization.

To quantify the effects of the surface to volume ratio, the total activation energy for the particle ($E_{a,NP}$) can be expressed as a combination of surface and bulk contributions:

$$E_{a,NP} = E_{a,B}\left[\frac{D-2d}{D}\right]^3 + E_{a,S}\left[1-\left[\frac{D-2d}{D}\right]^3\right] \quad (1)$$

where $E_{a,NP}$ is the energy of activation of the nanoparticle, $E_{a,B}$ is the energy of activation of the bulk material, $E_{a,S}$ is the energy of activation of the surface material, D is the size of the nanoparticle, and d the thickness of the layer contributing as surfacelike material. The depth at which the material shows surface behavior must be directly related to the rigidity of the lattice, a parameter intrinsic to the nature of the material. As a consequence, for a given compound, d should be the same for all particle sizes. In the bulk material, as the amount of surface becomes negligible, the bulk volume term tends to unity. Similar analyses have been applied to help understand related phenomena that are expected to have different rates at the surface and bulk, such as size-dependent magnetism in nanoparticles, where a significant increase in surface area induces preponderant surface-canting effects and therefore increases the magnetization.[58]

A kinetic model has been derived from the second-order reaction rate equation. Additional terms corresponding to the fraction of isomerized material at $t = 0$ and at equilibrium were introduced to account for the observation that we are monitoring a portion of the solid-state transformation (Supporting Information). Predictions shown as solid lines in Figure 4 were generated using the E_a values calculated from the FTIR analysis and the kinetic model. The generated lines are in good agreement with the data and allow the extraction of pre-exponential coefficients, α, corresponding to the material and common to the nanocrystals and bulk samples.

Considering the measured activation energy of compound **1** as an estimate of $E_{a,B}$, eq 1 can be used to calculate the thickness of the surface contribution, d, for both the 50 and 30 nm particles with E_a = 28 and 22 kJ·mol^{-1}, respectively. The analysis gives d = 6 ± 1 nm, with a mean value of 14 kJ·mol^{-1} for $E_{a,S}$, providing an estimate of the spatial boundary between the surface and core regimes of the linkage isomerism kinetics.

The length scale of the surface behavior has been further confirmed by the synthesis of ultrasmall nanocrystals (2 nm), behaving like surface material. Immediately after isolation of the sample, the FTIR spectrum showed a very large band indicating that the linkage isomerism already occurred in the material to a large extent (Supporting Information). The phenomenon was quantified at 255, 298, and 310 K, giving E_a = 11 kJ·mol^{-1} for 2 nm nanoparticles. This result supports the idea that nanocrystals in the 2−10 nm diameter range behave like surface material with E_a small enough for the linkage isomerism to take place rapidly at room temperature.

The depth of surface effects observed here for iron hexacyanochromate nanoparticles can be compared to that of other Prussian blue analogues. Pajerowski et al.[59] reported the limits of photoinduced magnetism in nanosized cobalt hexacyanoferrate Prussian blue analogue particles by correlating the extent of the photomagnetic response with the intrinsic particle size distributions of different samples. The results establish a minimum size of ∼10 nm required to observe photoinduced magnetism. The similar length scales observed in the two different studies suggest a depth of 5−10 nm for chemical and structural reorganization at the surface of Prussian blue analogue solids.

■ CONCLUSIONS

Highly reproducible, iron(II) hexacyanochromate(III) nanocrystals are synthesized with face diagonals of 50, 30, and 2 nm. Linkage isomerism rates are determined as a function of time and particle size. The PXRD, magnetism, and FTIR data indicate that the rate of isomerization increases while the particle size decreases. A kinetic study of the linkage isomerism at different temperatures shows the evolution of E_a with the size of the particles. Using the measured thermodynamic properties

dx.doi.org/10.1021/ic302764k | Inorg. Chem. 2013, 52, 4494−4501

and a simple two-component structural constraint hypothesis, the E_a for isomerization at surface sites is found to be significantly smaller than that for bulk sites.

■ ASSOCIATED CONTENT

Supporting Information

Magnetic measurements and FTIR at t = 0 and t = 91 h, solid-state second-order kinetic model, low-field region of magnetization, **M**, as a function of the applied field, μ_0**H**, showing the coercive field, **M** as a function of temperature, T, magnetic measurement procedures, activation energy as a function of particle size, and particle size distribution. This material is available free of charge via the Internet at http://pubs.acs.org.

■ AUTHOR INFORMATION

Corresponding Author

*E-mail: talham@chem.ufl.edu (D.R.T.), meisel@phys.ufl.edu (M.W.M.).

Present Addresses

[⊥]M.F.D.: The Sheikh Zayed Institute for Pediatric Surgical Innovation, Children's National Medical Center, 111 Michigan Ave., NW Washington, DC 20010.

[‖]NIST Center for Neutron Research, Gaithersburg, Maryland 20899-6012, United States.

Notes

The authors declare no competing financial interest.

■ ACKNOWLEDGMENTS

This work was supported by the National Science Foundation (NSF) through grants DMR-1005581 (D.R.T.) and DMR-1202033 (M.W.M.), and the National High Magnetic Field Laboratory (NHMFL) was supported via Cooperative Agreement NSF DMR-1157490 and by the State of Florida. We thank Ben Pletcher and Kerry Siebein at the University of Florida Major Analytical Instrument Center for HRTEM imaging and EDS analysis work. Additional support from the UF DSR Research Opportunity Fund is gratefully acknowledged.

■ REFERENCES

(1) Rosseinsky, D. R.; Glidle, A. *J. Electrochem. Soc.* **2003**, *150*, C641−C645.

(2) Mortimer, R. J.; Reynolds, J. R. *J. Mater. Chem.* **2005**, *15*, 2226−2233.

(3) Ko, J. H.; Yeo, S.; Park, J. H.; Choi, J.; Noh, C.; Son, S. U. *Chem. Commun.* **2012**, *48*, 3884−3886.

(4) Heydlauf, H. *Eur. J. Pharmacol.* **1969**, *6*, 340−344.

(5) Torad, N. L.; Hu, M.; Imura, M.; Naito, M.; Yamauchi, Y. *J. Mater. Chem.* **2012**, *22*, 18261−18267.

(6) Karyakin, A. A.; Puganova, E. A.; Budashov, I. A.; Kurochkin, I. N.; Karyakina, E. E.; Levchenko, V. A.; Matveyenko, V. N.; Varfolomeyev, S. D. *Anal. Chem.* **2004**, *76*, 474−478.

(7) Nossol, E.; Gorgatti, Z. A. J. *J. Mater. Chem.* **2012**, *22*, 1824−1833.

(8) Ferlay, S.; Mallah, T.; Ouahes, R.; Veillet, P.; Verdaguer, M. *Nature* **1995**, *378*, 701−703.

(9) Holmes, S. M.; Girolami, G. S. *J. Am. Chem. Soc.* **1999**, *121*, 5593−5594.

(10) Frye, F. A.; Pajerowski, D. M.; Park, J.-H.; Meisel, M. W.; Talham, D. R. *Chem. Mater.* **2008**, *20*, 5706−5713.

(11) Sato, O.; Iyoda, T.; Fujishima, A.; Hashimoto, K. *Science* **1996**, *272*, 704−705.

(12) Sato, O.; Einaga, Y.; Fujishima, A.; Hashimoto, K. *Inorg. Chem.* **1999**, *38*, 4405−4412.

(13) Escax, V.; Bleuzen, A.; Cartier dit Moulin, C.; Villain, F.; Goujon, A.; Varret, F.; Verdaguer, M. *J. Am. Chem. Soc.* **2001**, *123*, 12536−12543.

(14) Pejakovic, D. A.; Manson, J. L.; Miller, J. S.; Epstein, A. J. *Phys. Rev. Lett.* **2000**, *85*, 1994.

(15) Tokoro, H.; Ohkoshi, S.-i.; Hashimoto, K. *Appl. Phys. Lett.* **2003**, *82*, 1245−1247.

(16) Ohkoshi, S.-i.; Hashimoto, K. *J. Am. Chem. Soc.* **1999**, *121*, 10591−10597.

(17) Sato, O. *J. Solid State Electrochem.* **2007**, *11*, 773−779.

(18) Sato, O. *Acc. Chem. Res.* **2003**, *36*, 692−700.

(19) Yamamoto, T.; Umemura, Y.; Nakagawa, M.; Iyoda, T.; Einaga, Y. *Thin Solid Films* **2007**, *515*, 5476−5483.

(20) Papanikolaou, D.; Kosaka, W.; Margadonna, S.; Kagi, H.; Ohkoshi, S.-i.; Prassides, K. *J. Phys. Chem. C* **2007**, *111*, 8086−8091.

(21) Papanikolaou, D.; Margadonna, S.; Kosaka, W.; Ohkoshi, S.-i.; Brunelli, M.; Prassides, K. *J. Am. Chem. Soc.* **2006**, *128*, 8358−8363.

(22) Pajerowski, D. M.; Gardner, J. E.; Frye, F. A.; Andrus, M. J.; Dumont, M. F.; Knowles, E. S.; Meisel, M. W.; Talham, D. R. *Chem. Mater.* **2011**, *23*, 3045−3053.

(23) Coronado, E.; Gimenez-Lopez, M. C.; Korzeniak, T.; Levchenko, G.; Romero, F. M.; Segura, A.; Garcia-Baonza, V.; Cezar, J. C.; de Groot, F. M. F.; Milner, A.; Paz-Pasternak, M. *J. Am. Chem. Soc.* **2008**, *130*, 15519−15532.

(24) Coronado, E.; Gimenez-Lopez, M. C.; Levchenko, G.; Romero, F. M.; Garcia-Baonza, V.; Milner, A.; Paz-Pasternak, M. *J. Am. Chem. Soc.* **2005**, *127*, 4580−4581.

(25) Pajerowski, D. M.; Andrus, M. J.; Gardner, J. E.; Knowles, E. S.; Meisel, M. W.; Talham, D. R. *J. Am. Chem. Soc.* **2010**, *132*, 4058−4059.

(26) Dumont, M. F.; Knowles, E. S.; Guiet, A.; Pajerowski, D. M.; Gomez, A.; Kycia, S. W.; Meisel, M. W.; Talham, D. R. *Inorg. Chem.* **2011**, *50*, 4295−4300.

(27) Knowles, , E. S.;; Li, , C. H.;; Dumont, , M. F.;; Peprah, , M. K.;; Andrus, , M. J.;; Talham, , D. R.;; Meisel, , M. W. *Polyhedron* **2013**, , http://dx.doi.org/10.1016/j.poly.2013.03.019, , in press.

(28) Ohkoshi, S.; Tokoro, H.; Hashimoto, K. *Coord. Chem. Rev.* **2005**, *249*, 1830−1840.

(29) Ohkoshi, S.-i.; Fujishima, A.; Hashimoto, K. *J. Am. Chem. Soc.* **1998**, *120*, 5349−5350.

(30) Brown, D. B.; Shriver, D. F.; Schwartz, L. H. *Inorg. Chem.* **1968**, *7*, 77−83.

(31) House, J. E., Jr.; Bailar, J. C., Jr. *Inorg. Chem.* **1969**, *8*, 672−3.

(32) Arai, M.; Miyake, M.; Yamada, M. *J. Phys. Chem. C* **2008**, *112*, 1953−1962.

(33) Buschmann, W. E.; Ensling, J.; Gütlich, P.; Miller, J. S. *Chem.—Eur. J.* **1999**, *5*, 3019−3028.

(34) Nuida, T.; Hozumi, T.; Tokoro, H.; Hashimoto, K.; Ohkoshi, S.-i. *J. Solid State Electrochem.* **2007**, *11*, 763−772.

(35) Uemura, T.; Ohba, M.; Kitagawa, S. *Inorg. Chem.* **2004**, *43*, 7339−7345.

(36) Catala, L.; Brinzei, D.; Prado, Y.; Gloter, A.; Stephan, O.; Rogez, G.; Mallah, T. *Angew. Chem., Int. Ed.* **2009**, *48*, 183−187.

(37) Catala, L.; Volatron, F.; Brinzei, D.; Mallah, T. *Inorg. Chem.* **2009**, *48*, 3360−3370.

(38) Larionova, J.; Guari, Y.; Blanc, C.; Dieudonne, P.; Tokarev, A.; Guerin, C. *Langmuir* **2009**, *25*, 1138−1147.

(39) Layrac, G.; Tichit, D.; Larionova, J.; Guari, Y.; Guerin, C. *J. Phys. Chem. C* **2011**, *115*, 3263−3271.

(40) House, J. E.; Kob, N. E. *Inorg. Chem.* **1993**, *32*, 1053−1054.

(41) Bigelow, J. H., Bailar, J. C. Potassium Hexacyanochromate(III). *Inorganic Syntheses*; John Wiley & Sons, Inc.: Hoboken, NJ, 2007.

(42) Vaucher, S.; Fielden, J.; Li, M.; Dujardin, E.; Mann, S. *Nano Lett.* **2002**, *2*, 225−229.

(43) Yamada, M.; Sato, T.; Miyake, M.; Y., K. *J. Colloid Interface Sci.* **2007**, *315*, 369−375.

(44) Ohkoshi, S.; Einaga, Y.; Fujishima, A.; Hashimoto, K. *J. Electroanal. Chem.* **1999**, *473*, 245−249.

(45) Nakamoto, K. *Infrared Spectra of Inorganic and Coordination Compounds*; Wiley: New York, 1963
(46) Tolbert, S. H.; Alivisatos, A. P. *Annu. Rev. Phys. Chem.* **1995**, *46*, 595−625.
(47) Vaucher, S.; Li, M.; Mann, S. *Angew. Chem., Int. Ed.* **2000**, *39*, 1793−1796.
(48) Uemura, T.; Kitagawa, S. *J. Am. Chem. Soc.* **2003**, *125*, 7814−7815.
(49) Jinli, Y.; Yan, X.; Desheng, X. *Chem. Phys. Lett.* **2007**, *435*, 317−321.
(50) Frye, F. A.; Pajerowski, D. M.; Anderson, N. E.; Long, J.; Park, J.-H.; Meisel, M. W.; Talham, D. R. *Polyhedron* **2007**, *26*, 2273−2275.
(51) Kob, N. E.; House, J. E. *Transition Met. Chem. (Dordrecht, N eth.)* **1994**, *19*, 31−33.
(52) Clark, S. M.; Prilliman, S. G.; Erdonmez, C. K.; Alivisatos, A. P. *Nanotechnology* **2005**, *16*, 2813−2818.
(53) Qadri, S. B.; Skelton, E. F.; Hsu, D.; Dinsmore, A. D.; Yang, J.; Gray, H. F.; Ratna, B. R. *Phys. Rev. B* **1999**, *60*, 9191.
(54) Chen, C.-C.; Herhold, A. B.; Johnson, C. S.; Alivisatos, A. P. *Science* **1997**, *276*, 398−401.
(55) Cavalleri, A.; Tóth, C.; Siders, C. W.; Squier, J. A.; Ráksi, F.; Forget, P.; Kieffer, J. C. *Phys. Rev. Lett.* **2001**, *87*, 237401.
(56) Tolbert, S. H.; Alivisatos, A. P. *Science* **1994**, *265*, 373−376.
(57) Birk, J. P.; Espenson, J. H. *J. Am. Chem. Soc.* **1968**, *90*, 1153−1162.
(58) Morales, M. P.; Veintemillas-Verdaguer, S.; Montero, M. I.; Serna, C. J.; Roig, A.; Casas, L.; Martinez, B.; Sandiumenge, F. *Chem. Mater.* **1999**, *11*, 3058−3064.
(59) Pajerowski, D. M.; Frye, F. A.; Talham, D. R.; Meisel, M. W. *New J. Phys.* **2007**, *9*, 11.